

EventVAD: Training-Free Event-Aware Video Anomaly Detection

Yihua Shao
Peking University

Haojin He
Tsinghua University

Sijie Li
The University of Sheffield

Siyu Chen
University of Science and Technology
Beijing

Xinwei Long
Tsinghua University

Fanhu Zeng
Tsinghua University

Yuxuan Fan
Tsinghua University

Muyang Zhang
Tsinghua University

Ziyang Yan
University of Trento

Ao Ma
Institute of Computing Technology,
Chinese Academy of Science

Xiaochen Wang
University of Science and Technology
Beijing

Hao Tang
Peking University
haotang@pku.edu.cn

Yan Wang
Tsinghua University
wangyan@air.tsinghua.edu.cn

Shuyan Li
Queen's University Belfast
li-sy16@tsinghua.org.cn

ABSTRACT

Video Anomaly Detection (VAD) focuses on identifying anomalies within videos. Supervised methods require an amount of in-domain training data and often struggle to generalize to unseen anomalies. In contrast, training-free methods leverage the intrinsic world knowledge of large language models (LLMs) to detect anomalies but face challenges in localizing fine-grained visual transitions and diverse events. Therefore, we propose **EventVAD**, an event-aware video anomaly detection framework that combines tailored dynamic graph architectures and multimodal LLMs through temporal-event reasoning. Specifically, EventVAD first employs dynamic spatiotemporal graph modeling with time-decay constraints to capture event-aware video features. Then, it performs adaptive noise filtering and uses signal ratio thresholding to detect event boundaries via unsupervised statistical features. The statistical boundary detection module reduces the complexity of processing long videos for MLLMs and improves their temporal reasoning through event consistency. Finally, it utilizes a hierarchical prompting strategy to guide MLLMs in performing reasoning before determining final decisions. We conducted extensive experiments on the UCF-Crime and XD-Violence datasets. The results demonstrate that EventVAD with a 7B MLLM achieves *state-of-the-art* (SOTA) in training-free settings, outperforming strong baselines that use 7B or larger MLLMs.

CCS CONCEPTS

• **Do Not Use This Code** → **Generate the Correct Terms for Your Paper**; *Generate the Correct Terms for Your Paper*; Generate the Correct Terms for Your Paper; Generate the Correct Terms for Your Paper.

KEYWORDS

Multimodal Large Language Models, Vision-Language Model, Video Understanding, Video Anomaly Detection

1 INTRODUCTION

Leveraging multimodal large models (MLLMs) [25, 66] to comprehend details in videos is crucial for multimedia [57]. Among them, Video Anomaly Detection (VAD) [31] aims to locate the anomaly frames accurately [64, 65]. Before the advent of large language models (LLMs) [5, 9, 24, 46, 69], supervised training-based methods [36, 40, 54, 55, 61] enable neural networks to achieve greater precision 90% on specific datasets. However, these methods struggle to generalize in unseen settings [37] and require in-domain fine-tuning in new scenarios. Meanwhile, there are also one-class supervision (normal only) [40, 51] and unsupervised training strategies [62]. Due to the lack of effective labels, these methods cannot achieve the same performance as supervised approaches.

With the advancement of MLLMs [5, 24, 49, 68, 69], models such as LLaVA [24] have enabled coarse-grained localization of anomalous frames through frame-by-frame understanding. However, these methods lack temporal understanding capabilities, which results in a lack of consistent understanding of videos. As for training-free methods, LAVAD [63] leverages a combination of visual question-answering models [18] and LLMs [9] to score anomalous frames, thus achieving the localization of such frames. LAVAD utilizes four image question-answering models to analyze each frame while relying on an LLM with at least 13 billion parameters for anomaly scoring. This leads to an inefficient framework [34, 35, 67] and may lead to long-tail problems.

Permission to make digital or hard copies of all or part of this work for personal or classroom use is granted without fee provided that copies are not made or distributed for profit or commercial advantage and that copies bear this notice and the full citation on the first page. Copyrights for components of this work owned by others than the author(s) must be honored. Abstracting with credit is permitted. To copy otherwise, or republish, to post on servers or to redistribute to lists, requires prior specific permission and/or a fee. Request permissions from permissions@acm.org.

Conference acronym 'XX, October 27–31, 2025, Dublin, Ireland

© 2025 Copyright held by the owner/author(s). Publication rights licensed to ACM.

ACM ISBN 978-1-4503-XXXX-X/2018/06...\$15.00

<https://doi.org/XXXXXXX.XXXXXXX>

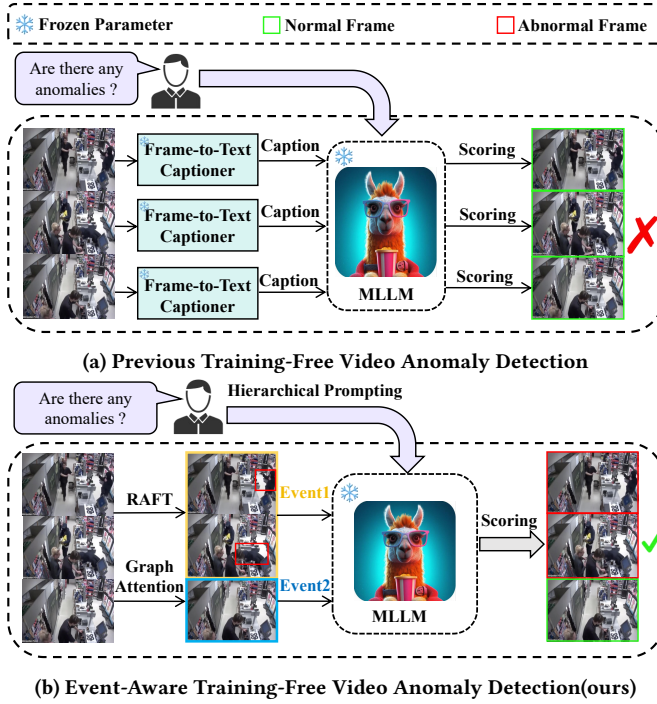


Figure 1: Comparison of current video anomaly detection frameworks. Fig. 1a Existing training-free methods struggle to localize fine-grained abnormal frames. In contrast, our framework (Fig. 1b) segments events to enhance event consistency and fine-grained abnormal detection.

Inspired by LAVAD [63], we find that training-free approaches are unable to fully localize anomalous events in videos, leading to biases in subsequent LLM scoring. To address these issues, we propose a training-free framework **EventVAD**, which segments long videos into short videos to enhance event consistency during MLLM understanding. EventVAD first extracts features from each frame using the ViT-B/16 of EVA-CLIP [41], and then enhances inter-frame features using RAFT optical flow [42] to capture fine-grained features. For temporal features, EventVAD employs its tailored Graph Attention mechanism to aggregate temporal features. This enhances the temporal consistency of events, making it more conducive to boundary detection and event segmentation. Finally, EventVAD inputs the segmented events into an MLLM [5] for scoring, to determine the anomaly level of each frame.

We evaluate EventVAD on UCF-Crime [40] and XD-Violence [55] datasets. Experimental results demonstrate that EventVAD achieves *state-of-the-art* (SOTA) compared to training-free, self-supervised, and one-class supervised methods, and even outperforms some weak-supervised methods. Notably, we have reduced the model parameters from over 13 billion to 7 billion, significantly reducing storage and inference costs.

Our contributions can be summarized as follows:

- We propose a training-free event-aware video anomaly detection framework, **EventVAD**, which reduces errors in MLLMs scoring by segmenting events into short events to enhance videos' temporal consistency.

- We design a Graph Attention mechanism to model features across multiple frames. By incorporating RAFT optical flow to enhance frame features, Graph Attention enables more accurate event boundary detection and event segmentation.
- EventVAD achieves *SOTA* performance among training-free, unsupervised, and one-class methods on both UCF-Crime and XD-Violence datasets, and even surpasses some weakly supervised methods. Additionally, EventVAD compresses the model's parameters from 13 to 7 billion, significantly reducing computational costs.

2 RELATED WORK

2.1 Video Anomaly Detection

Video Anomaly Detection (VAD) has gained significant attention in recent years due to its wide range of applications aimed at identifying anomalous events in video sequences [22, 29, 31, 40]. Existing approaches can be broadly categorized into training-based and training-free paradigms. Recent research in VAD has focused on weakly supervised training paradigms, unsupervised training paradigms and training-free paradigms. Weakly-supervised VAD leverages video-level labels to localize frame-level anomalies, avoiding the prohibitive cost of manual frame annotation [15, 17, 21, 40, 45, 54]. Most of these methods utilize 3D convolutional neural networks for feature learning and are trained with multi-instance learning (MIL) loss [32, 56, 58, 59]. Unsupervised VAD methods do not require any labeled data and instead rely on the inherent structure of normal video data to detect anomalies [43, 44, 47, 48, 62]. Among them, using generative models to capture normal data patterns in videos performs best in unsupervised video anomaly detection, especially in complex scenes and time series data processing. However, these training-based approaches require data collection and model retraining in practical deployment scenarios. As the first language-based method for training-free VAD using LLMs, LAVAD [63] leverages modality-aligned MLLMs to query and enhance the anomaly scores generated by large language models (LLMs). Based on this, MCANet [6] is a training-free video anomaly detection framework that dynamically generates multi-modal text descriptions and analyzes them for efficient anomaly detection by fusing visual language models, audio language models and large language models. Building upon these innovations, through temporal segmentation into discrete event units, EventVAD significantly mitigates error propagation in long-form video analysis, reducing false detection rates.

2.2 Video Understanding

Video understanding tasks have been driven by the integration of MLLMs with temporal modeling. Early approaches in Video Large Language Models (Video-LLMs) [2, 13, 20, 23, 26, 28, 70] primarily adopted vision-language adapters from Image-LLMs, such as cross-attention [1], Q-former [18, 60, 73], linear projection [3, 25, 52] and dynamic visual tokenizer [14]. These adapters bridge visual features with language models by compressing frame-level representations into fixed-length tokens. For instance, Video-LLaMA [70] employs a video-specific Q-Former to aggregate temporal features, while Video-ChatGPT [28] incorporates spatial and temporal pooling layers to enhance frame-level reasoning. Recent works like

VTimeLLM [12] and CogVLM2 [11] propose boundary-aware training and timestamp-aware encoding, respectively, to address the problem of the limited effective context length of LLM for long video processing and redundancy in processing similar frames. The integration of multimodal alignment techniques has further expanded video understanding capabilities. Models like ImageBind [8] unify embeddings across six modalities into a shared latent space, enabling zero-shot cross-modal retrieval. This approach has been widely adopted in frameworks such as PandaGPT [39], where audio streams are aligned with visual features via pre-trained encoders. However, these methods prioritize modality fusion over temporal-audio synchronization, limiting their ability to correlate dynamic events with acoustic cues. EventVAD leverages video LLMs to analyze segmented events, generating frame-level anomaly scores for precise temporal localization of abnormal content.

3 METHODOLOGY

Given an input video sequence $\mathcal{V} = \{\mathbf{I}_t\}_{t=1}^T$ with T frames, our objective is to detect anomaly frames. $\{a_t\}_{t=1}^T$ are anomaly indicators, where $a_t \in \{0, 1\}$ represents the binary abnormality status for frame \mathbf{I}_t . The overall pipeline is shown as Fig 2, which consists of four components. Our method first constructs a dynamic graph with multimodal temporal decay, where nodes represent fused frame features and edges encode spatiotemporal correlation. Then, graph attention propagation refines node features through orthogonally constrained messaging. The enhanced features are processed by the Statistical Boundary Detection module to identify event transformations and obtain event boundaries through discontinuity analysis. Finally, event-centric scoring uses semantic cues to assess anomalies within detected event units.

3.1 Event-Aware Dynamic Graph Construction

Node Feature Construction. To address the inherent limitations of static graphs in capturing dynamic video events and the slow training speed of graph neural networks [33], we propose a dynamic spatiotemporal graph model based on video frames. Our model jointly optimizes multimodal node representations and time-sensitive edge connections. The proposed dynamic spatiotemporal graph model $G = (F, E)$ introduces adaptive node representations through multimodal feature interaction. The vertex set F corresponds to video frame units with enhanced feature encoding, while edges in E are dynamically established using cross-modal similarity metrics.

The nodal feature representation integrates a dual-stream architecture that combines semantic and motion patterns. As shown in Eq. (1), the semantic branch employs CLIP [30] to generate discriminative embeddings via L2-normalization.

$$f_i^{\text{clip}} = \frac{\phi_{\text{CLIP}}(\mathbf{I}_i)}{\|\phi_{\text{CLIP}}(\mathbf{I}_i)\|_2}, \quad (1)$$

where ϕ_{CLIP} generates 512-dimensional semantic embeddings ($\mathbf{s}_i \in \mathbb{R}^{512}$). This explicit normalization amplifies feature discontinuities between frames, a critical component for detecting semantic-level event boundaries.

The motion branch captures temporal dynamics using optical flow processing. This branch is formulated as Eq. (2):

$$f_i^{\text{flow}} = \mathbf{P}^\top \mathbb{E}[\mathbf{o}_{i \rightarrow i-1}], \quad (2)$$

where $\mathbf{o}_{i \rightarrow i-1} \in \mathbb{R}^{H \times W \times 2}$ represents the optical flow fields from RAFT [42]. The projection matrix $\mathbf{P} \in \mathbb{R}^{2 \times 128}$ maps high-dimensional flow statistics to compact motion codes ($\mathbf{m}_i \in \mathbb{R}^{128}$). This dimensionality reduction improves the discriminability of motion patterns while preserving temporal coherence.

The fused node representation for the graph vertex $v_i \in F$ is calculated using Eq. (3):

$$\mathbf{f}_i = \alpha f_i^{\text{clip}} \oplus (1 - \alpha) f_i^{\text{flow}}, \quad (3)$$

where the semantic-motion fusion coefficient $\alpha = 0.75$ and the eigenvector \mathbf{f}_i integrate semantic and motion constraints to precisely define event transformation boundaries.

Temporal Decay Adjacency Matrix. Fundamentally, analyzing the temporal evolution of video content requires integrating spatio-temporal variations across components. To model node relationships, we construct a dynamic graph with time decay.

The time decay adjacency matrix E is defined as Eq. (4):

$$E_{ij} = \frac{\alpha \cdot \cos(f_i^{\text{clip}}, f_j^{\text{clip}}) + (1 - \alpha) \cdot \exp(-\|f_i^{\text{flow}} - f_j^{\text{flow}}\|)}{1 + \gamma \cdot |i - j|}. \quad (4)$$

where the semantic-motion fusion coefficient $\alpha = 0.75$ is shared with the node usage coefficient. To emphasize short-term correlations and suppress long-term ones, our model combines multimodal similarity between frames i and j in the numerator. In the denominator, we introduce a γ time decay factor to penalize remote associations, which diminish with temporal distance.

3.2 Graph Attention Networks Propagation

To improve frame-by-frame representation while preserving temporal consistency, we propose a training-free attention mechanism based on orthogonal feature projection in spacetime. This mechanism amplifies segment contrast through graph-guided message passing, enhancing event boundary distinguishability. Our approach builds upon graph attention networks [50] with orthogonal constraints.

Given the propagated node features $\mathbf{F}^{(0)} = [\mathbf{f}_1, \dots, \mathbf{f}_n]^\top \in \mathbb{R}^{n \times d}$ from Section 3.1, we project the features into orthogonal subspaces to prevent dimension collapse as Eq (5),

$$\begin{cases} \mathbf{Q} = \text{QR}\{\mathcal{N}(0, 1)^{d \times k}\} \\ \mathbf{K} = \text{QR}\{\mathcal{N}(0, 1)^{d \times k}\} \\ \mathbf{V} = \text{QR}\{\mathcal{N}(0, 1)^{d \times d}\} \end{cases}, \quad (5)$$

where $\text{QR}(\cdot)$ ensures orthonormal columns via QR decomposition, $d = 640$ is the fused feature dimension, and $k = 64$ is the projected dimension. These fixed orthogonal matrices maximize feature retention.

For node f_i the attention weight for neighbor f_j in the dynamic graph is calculated as:

$$\text{Atten}_{ij} = \text{Softmax}\left(\frac{(\mathbf{f}_i \mathbf{Q})(\mathbf{f}_j \mathbf{K})^\top}{\sqrt{d_a}}\right)(\mathbf{f}_j^{(t)} \mathbf{V}). \quad (6)$$

The indicator function $\mathbb{E}_{(i,j)}$ adheres to temporal connectivity from Section 3.1, ensuring attention respects event-induced topology. This constraint prevents attention dispersion to irrelevant

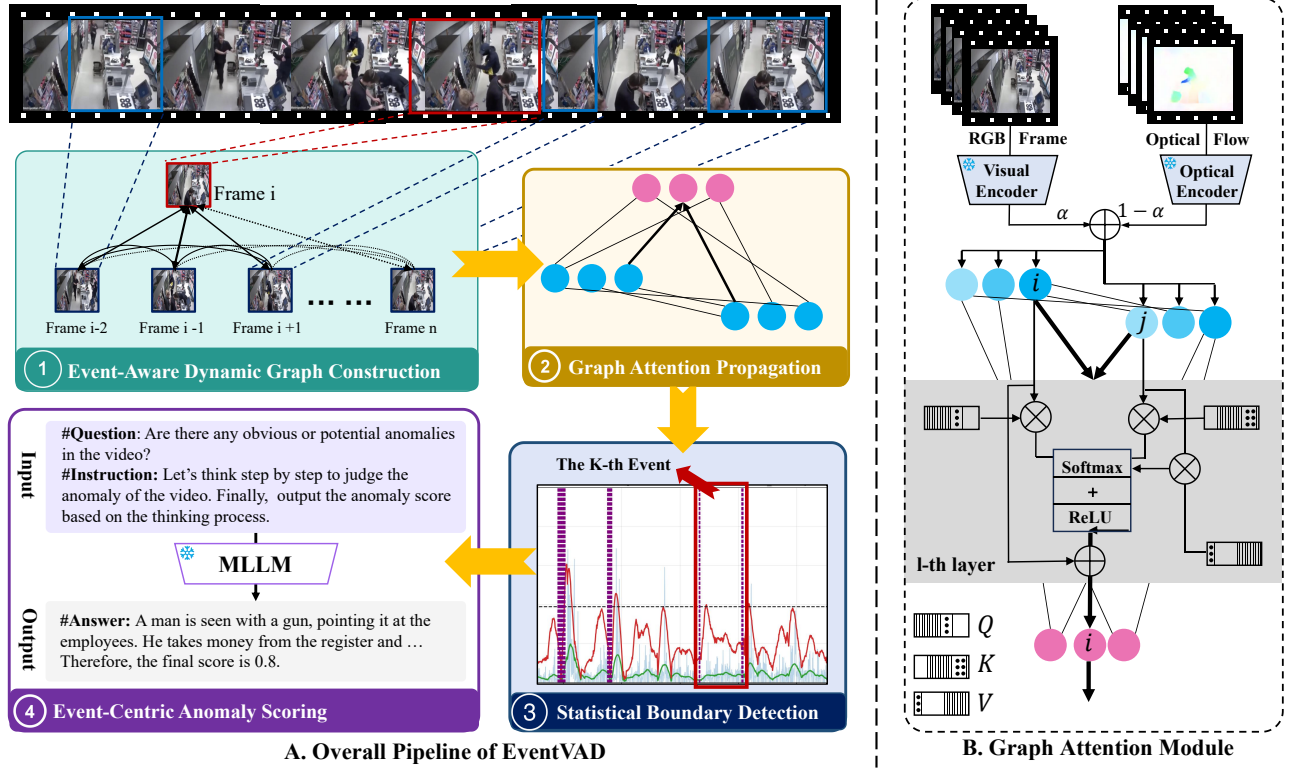


Figure 2: Overall Pipeline of EventVAD. The Dynamic Graph Construction stage establishes spatiotemporal correlations using multimodal node features and time-decayed edges. Next, the Graph Attention Propagation refines node representations via orthogonally constrained message passing to enhance event transitions. Subsequently, the Statistical Boundary Detection stage identifies event boundaries by combining composite divergence metrics with adaptive thresholding. Finally, the Event-Centric Scoring stage employs MLLMs to evaluate anomaly likelihoods within semantically coherent event units. This architecture hierarchically analyzes video content from low-level feature dynamics to high-level event semantics, overcoming the limitations of frame-level methods through temporally aware event decomposition.

frames. Features update iteratively via:

$$\mathbf{f}_i^{(t+1)} = \mathbf{f}_i^{(t)} + \sum_{j \in \mathcal{N}_i} \text{Atten}_{ij} \cdot \mathbb{E}_{(i,j)}. \quad (7)$$

After each iteration, features are centered as:

$$\mathbf{f}_i^{(t+1)} \leftarrow \mathbf{f}_i^{(t+1)} - \frac{1}{|F|} \sum_{k \in F} \mathbf{f}_k^{(t+1)}. \quad (8)$$

Through iterative graph attention updates, feature propagation maintains global divergence and local consistency, preserving relative differences critical for anomaly detection.

3.3 Statistical Boundary Detection

For enhanced graph attention network features, we propose a statistical boundary detection mechanism to identify event transitions via temporal discontinuity analysis.

For consecutive frames $(i, i+1)$, we compute a composite divergence metric:

$$s_i = \underbrace{\|\mathbf{f}_{i+1} - \mathbf{f}_i\|_2^2}_{\text{Feature Magnitude Jump}} + \underbrace{\left(1 - \frac{\mathbf{f}_i^\top \mathbf{f}_{i+1}}{\|\mathbf{f}_i\| \|\mathbf{f}_{i+1}\|}\right)}_{\text{Cosine Dissimilarity}}, \quad (9)$$

where the squared L2 term amplifies abrupt feature-space jumps, and the cosine term detects directional changes in the manifold. This dual strategy captures amplitude and directional discontinuities caused by anomalies.

The raw dissimilarity score s_i includes high-frequency noise from camera shake or minor motion. To suppress noise while preserving true boundaries, we apply a Savitzky-Golay filter with a window width $w = 60$, defined as:

$$\tilde{s}_i = \frac{1}{w} \sum_{k=-w/2}^{w/2} a_k s_{i+k}, \quad (10)$$

where a_k derives from a quadratic polynomial fit, retaining true discontinuities.

For the smoothed signal \tilde{s}_i , we compute a moving average:

$$\mu_i = \frac{1}{w} \sum_{k=i-\lfloor w/2 \rfloor}^{i+\lfloor w/2 \rfloor} \tilde{s}_i. \quad (11)$$

The signal ratio r_i is then calculated as:

$$r_i = \frac{\tilde{s}_i}{\mu_i}, \quad (12)$$

where equal window weights suppress transient fluctuations, enhancing noise robustness.

To mitigate outlier sensitivity from occlusions or jitter, we use median absolute deviation for adaptive thresholding:

$$\text{MAD}(r_i) = \text{median}(|r_i - \text{median}(r_i)|), \quad (13)$$

$$M = \text{median}(r_i) + k \times \text{MAD}(r_i). \quad (14)$$

Adjusting $k = 3$ aligns with the 3σ principle [16], capturing 99.7% of normal variation. Boundaries are identified when $r_i > M$.

Finally, adjacent boundary points are merged to prevent over-segmentation, refining event boundary accuracy.

3.4 Event-Centric Anomaly Scoring

Existing video anomaly detection methods [63] often rely on discrete frame-level analysis or global video processing. However, their non-adaptive segmentation mechanisms face a critical trade-off: overly short temporal fragments lose contextual information, while excessively long units weaken spatial feature representation. This limitation hinders visual language models' ability to interpret videos effectively.

To address this, we construct event semantic units as spatiotemporal primitives, creating an optimized feature representation framework for visual-language models [25]. For event unit analysis, we propose a semantic-driven hierarchical prompting framework. This framework directs multimodal large language models to produce structured outputs: first generating video content descriptions and then deriving anomaly scores. When processing a video, the multimodal large language models initially generate descriptive text by identifying surface and latent semantic features. It subsequently outputs an anomaly score based on this description, enabling cross-modal evaluation against predefined criteria.

By implementing a two-stage reasoning framework, we establish a self-correction mechanism. This architecture allows systematic score derivation through video content analysis, ensuring contextual relevance and reducing scoring inaccuracies.

4 EXPERIMENT

We rigorously evaluated EventVAD in two benchmarks and compared it to state-of-the-art video anomaly detection methods. In Section 4.1, we detail the experimental setup in terms of data sets and performance metrics, then present and discuss the results in Section 4.2, and finally, the ablation experiments in Section 4.3.

4.1 Experiment Setting

Setting Up. The encoder uses a dual-branch architecture that combines visual semantics and motion representation, using the CLIP ViT-B/16 model [30] to generate 512-dimensional semantic embeddings, while optical flow features are extracted by the pre-trained

RAFT model to generate 128-dimensional vectors, with frame pairs processed at intervals $\Delta t=1$, and bilinear interpolation for spatial alignment to maintain resolution consistency. The scoring architecture was implemented using VideoLLaMA2.1-7B-16F [5] as the backbone model. The key hyperparameter time decay factor is set to $\alpha = 0.6$, the semantic-motion fusion coefficient is set to $\beta = 0.75$, and the graph attention propagation is only a single iteration. All experiments were conducted on a single NVIDIA A800 (80GB) GPU. **Datasets.** We evaluate EventVAD against two widely adopted video anomaly detection benchmarks, UCF-Crime [40] and XD-Violence [55]. The details of datasets are as Appendix A.1.

Evaluation Metrics. For the UCF-Crime dataset, we employ frame-level AUC-ROC (Area Under the Receiver Operating Characteristic Curve). For the XD-Violence dataset, we also employ AP (Average Precision) as primary metrics to align with standard VAD evaluation protocols. The detail can be seen in Appendix A.2.

4.2 Main Results

Results on UCF-Crime. Since the UCF-Crime data come from the real shooting scene of the camera, the similarity between events in the same video is high. It is more challenging when the model divides the events. As shown in Tab. 1, EventVAD surpasses all training-free methods to *state-of-the-art* (SOTA) and outperforms LAVAD by nearly 4%. Compared to LAVAD, EventVAD's foundational model is Video-Llama2 [5] with a parameter count of 7b, which has a significant decrease in the overall parameter of the model. Also, EventVAD outperforms all unsupervised and one-class methods, as well as some weakly supervised methods on UCF-Crime.

By analyzing the results, we found that since the other methods ignore dividing the video, different model parameter sizes cannot achieve accurate localization when dealing with long videos. This suggests that EventVAD's approach of dividing events and then scoring event anomalies can effectively mitigate the model's inability to achieve anomaly detection for long videos. Even in noisy scenarios, EventVAD demonstrates robust detection capability under challenging conditions with both rare abnormal samples (low occurrence rate <5%) and significant visual noise.

Results on XD-Violence. Since the XD-Violence datasets are all derived from video recordings, the videos are clearer, and there is less noise in the picture. As shown in Tab. 2, EventVAD's AP and AUC on this dataset are almost 5% higher than the current training-free SOTA LAVAD [63]. Also, EventVAD anomaly detection capability surpasses all one-class and unsupervised methods. This indicates that EventVAD is not only suitable for low-resolution scenarios but also applicable to high-resolution scenarios. Even though EventVAD has significantly fewer model parameters than LAVAD, its performance shows a substantial improvement compared to LAVAD. This can significantly reduce computational and deployment costs for the model.

After analyzing the samples that LAVAD failed to detect, we found that the current model performs poorly in long-video detection. Additionally, many abnormal events only occupy a small portion of the frame, making it difficult for the model to achieve precise localization. Moreover, compared to LAVAD, EventVAD's

Method	Backbone	Supervised	AUC (%)
Sultani <i>et al.</i> [40]	C3D-RGB	Weakly Supervised	75.41
Sultani <i>et al.</i> [40]	I3D-RGB	Weakly Supervised	77.92
IBL [71]	C3D-RGB	Weakly Supervised	78.66
GCL [62]	ResNext	Weakly Supervised	79.84
GCN [72]	TSN-RGB	Weakly Supervised	82.12
MIST [7]	I3D-RGB	Weakly Supervised	82.30
Wu <i>et al.</i> [55]	I3D-RGB	Weakly Supervised	82.44
CLAWS [61]	C3D-RGB	Weakly Supervised	83.03
RTFM [45]	VideoSwin-RGB	Weakly Supervised	83.31
RTFM [45]	I3D-RGB	Weakly Supervised	84.03
Wu & Liu <i>et al.</i> [54]	I3D-RGB	Weakly Supervised	84.89
MSL [21]	I3D-RGB	Weakly Supervised	85.30
MSL [21]	VideoSwin-RGB	Weakly Supervised	85.62
S3R [53]	I3D-RGB	Weakly Supervised	85.99
MGFN [4]	VideoSwin-RGB	Weakly Supervised	86.67
MGFN [4]	I3D-RGB	Weakly Supervised	86.98
SSRL [17]	I3D-RGB	Weakly Supervised	87.43
CLIP-TSA [15]	ViT	Weakly Supervised	87.58
SVM [40]	-	One Class	50.00
SSV [38]	-	One Class	58.50
BODS [51]	I3D-RGB	One Class	68.26
GODS [51]	I3D-RGB	One Class	70.46
GCL [62]	ResNext	Unsupervised	74.20
Tur [47]	ResNet	Unsupervised	65.22
Tur [48]	ResNet	Unsupervised	66.85
DyAnNet [44]	I3D	Unsupervised	79.76
Blip2 [18]	ViT	Training Free	46.42
ZS CLIP [30]	ViT	Training Free	53.16
ZS ImageBind (Image) [8]	ViT	Training Free	53.65
ZS ImageBind (Video) [8]	ViT	Training Free	55.78
LLaVA-1.5 [24]	ViT	Training Free	72.84
Video-Llama2 [70]	ViT	Training Free	74.42
LAVAD [63]	ViT	Training Free	78.33
EventVAD (Ours)	ViT	Training Free	82.03

Table 1: Results on the UCF-Crime dataset. EventVAD substantially outperforms the current training-free SOTA LAVAD and all one-class and unsupervised methods. Compared to some weakly-supervised approaches, EventVAD also demonstrates superior performance.

prompt setup is very straightforward. We achieve multi-stage reasoning in MLLM through hierarchical prompting to enhance its scene-understanding capability.

Visual Analysis. As shown in Fig. 3, using a UCF-Crime video sample as an example, we demonstrate a comprehensive visualization of abnormal and normal sequences by the graph attention propagation process.

Fig. 3 reveals fundamental differences in the modeling of the temporal relationship between normal and abnormal sequences. Both the Subgraph 3a and Subgraph 3c show chaotic inter-frame connections, with low discriminative long-distance dependence. After the attention propagation of the applied graph, subgraphs (c) and (d) clearly show strengthened connections between adjacent frames, and the pseudo-correlation with the distant frame is suppressed. In particular, Subgraph 3d as a whole presents a relatively uniform inter-frame weight, but Subgraph 3c has a unique cluster of low weights around frames 965-975, which corresponds to the actual boundary division.

This actually verifies how the propagation process of our graph attention acts as a feature contrast amplifier, with the help of which the Statistical Boundary Detection module can convert the amplified signal difference into an accurate event boundary.

METHOD	BACKBONE	Supervised	AP (%)	AUC (%)
Wu <i>et al.</i> [55]	C3D-RGB	Weakly Supervised	67.19	-
Wu <i>et al.</i> [55]	I3D-RGB	Weakly Supervised	73.20	-
MSL [21]	C3D-RGB	Weakly Supervised	75.53	-
Wu and Liu [54]	I3D-RGB	Weakly Supervised	75.90	-
RTFM [45]	I3D-RGB	Weakly Supervised	77.81	-
MSL [21]	I3D-RGB	Weakly Supervised	78.28	-
MSL [21]	VideoSwin-RGB	Weakly Supervised	78.58	-
S3R [53]	I3D-RGB	Weakly Supervised	80.26	-
MGFN [4]	I3D-RGB	Weakly Supervised	79.19	-
MGFN [4]	VideoSwin-RGB	Weakly Supervised	80.11	-
Hasan <i>et al.</i> [10]	AE ^{RGB}	One Class	-	50.32
Lu <i>et al.</i> [27]	Dictionary	One Class	-	53.56
BODS [51]	I3D-RGB	One Class	-	57.32
GODS [51]	I3D-RGB	One Class	-	61.56
RareAnom [43]	I3D-RGB	Unsupervised	-	68.33
Blip2 [18]	ViT	Training Free	10.89	29.43
ZS CLIP [30]	ViT	Training Free	17.83	38.21
ZS ImageBind (Image) [8]	ViT	Training Free	27.25	58.81
ZS ImageBind (Video) [8]	ViT	Training Free	25.36	55.06
LLaVA-1.5 [24]	ViT	Training Free	50.26	79.62
Video-Llama2 [70]	ViT	Training Free	53.57	80.21
LAVAD [63]	ViT	Training Free	60.02	82.89
EventVAD (Ours)	ViT	Training Free	64.04	87.51

Table 2: Results on the XD-Violence dataset. EventVAD achieves significantly superior performance over the current training-free SOTA LAVAD on the XD-Violence dataset, outperforming all one-class and unsupervised methods.

Boundary Detection Visualization. As shown in Fig. 4, we visualize the boundary detection of all frames of these video samples. The light blue curve represents the original signal used for segmentation, the green curve represents the signal after being smoothed by Savitzky-Golay filtering, the red curve represents the change in the ratio of the smoothed signal within the window to the average line of the corresponding window, the black horizontal line represents the adaptive threshold, and the purple horizontal line represents the detected boundary.

For different types of videos, there are usually different event boundary patterns. Normal video sequences have fewer events due to their good consistency, while abnormal videos have the opposite. The difference between Subgraph 4a and Subgraph 4b validates that our framework can take advantage of this feature to obtain clear boundary points at different boundary densities when the score threshold is set to 2, thus achieving a robust distinction between normal time coherence and anomalous discontinuity.

In the Subgraph 4a, for frames 965-975 of the video, our framework can effectively capture the key boundary detection patterns after the graph attention propagation, which also quantitatively verifies the subsequent boundary detection process of the Subgraph 3b. In addition, the framework exhibits noise elasticity when dealing with high variance clips, such as 1200 to 1300 frames of video, and maintains some sensitivity to interframe variations in overall signal-stable clips, such as 1750 to 1900 frames of video.

Qualitative Results To intuitively demonstrate EventVAD’s capabilities, we visually compare its performance against LAVAD by selecting failure cases from both the UCF-Crime and XD-Violence datasets for qualitative analysis.

For anomalous samples, as shown in Fig. 5a, the video is a long sequence with over 2,500 frames, and the anomaly (robbery) is primarily concentrated in the lower-right corner of the footage. Therefore, most methods like LAVAD [63] struggle to detect such

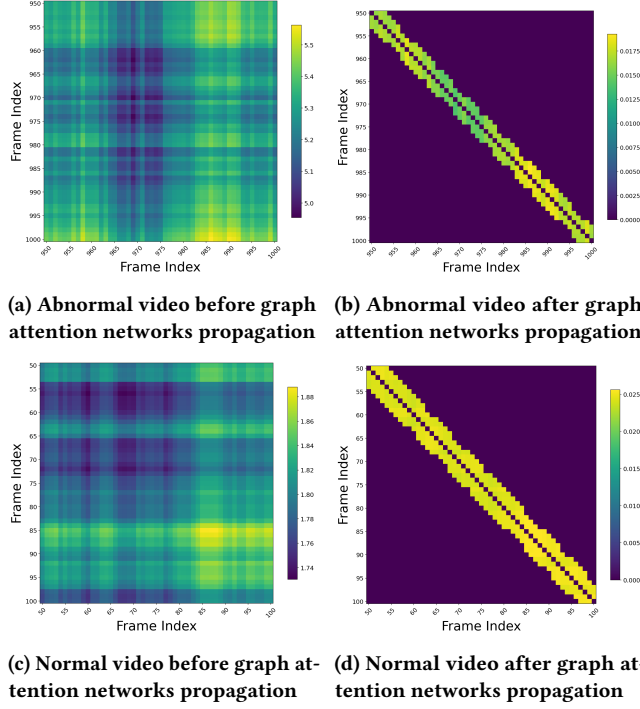


Figure 3: Graph attention propagation visualization analysis. We take the abnormal and normal video samples in the UCF-Crime dataset to visualize the inter-frame relationship before and after the application of Graph Attention Propagation. The heat maps show the change of the weight relationship between frames in the corresponding frame interval.

subtle anomalies. Although EventVAD’s segmentation of event boundaries (start/end points) lacks precision, it effectively identifies the core segments of events. As shown in Fig. 5c, despite the visual prominence of the main subjects in the video, environmental interference can occasionally cause them to disappear from view. EventVAD segments videos into distinct events and leverages event consistency to enable precise anomaly localization within each event, effectively reducing false detections by the model.

For normal samples, as shown in Fig. 5b and Fig. 5d, Fig. 5b exhibits significant blurriness with poorly defined subjects, which poses substantial challenges for QA models like Blip [18, 19] in performing accurate detection. Fig. 5d exceeds 1,400 frames in length, presenting significant detection challenges for LLMs [25, 46]. Using an event-aware approach, EventVAD optimizes video length for LLM input through event consistency. Even for lengthy videos, consistent events enable the LLM to achieve comprehensive anomaly detection by analyzing only the initial frames, thereby avoiding length-induced misjudgments.

4.3 Ablation Study

To validate the design of the EventVAD, we conduct ablation studies and evaluate the contribution of the individual components. For a fair comparison, all ablation experiments are performed using the UCF-Crime [40] evaluation dataset.

Efficiency-Accuracy Trade-off. Since the foundational model parameters of the original LAVAD is 13 billion, we will explore the

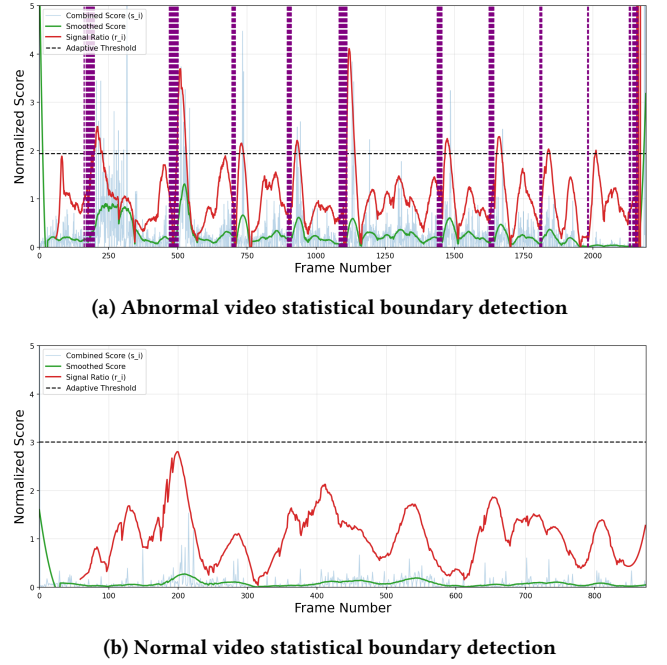


Figure 4: Statistical boundary detection visual analysis. We use samples from the UCF-Crime dataset as an example to visualize the boundary detection process of abnormal and normal videos.

impact of model size on the framework’s performance. As shown in Tab. 3, we first aligned the base model parameters of LAVAD and EventVAD. When both base models used Llama2 [46], we found that increasing LAVAD’s model parameters could selectively enhance its anomaly detection capability. Although EventVAD also showed some improvement with larger model parameters, the gain was less pronounced compared to LAVAD. When using the 7B-parameter Video-Llama2 [5], EventVAD achieved an AUC of 82.03%, which is 3.69% higher than the 13B-parameter LAVAD baseline. This validates the effectiveness of our event-centric architecture and reveals its ability to reduce the reliance on parametric scaling through methodological innovation. The results on the XD-Violence dataset can be seen in Appendix A.3.

Moreover, the results demonstrate that although LAVAD employs cosine similarity for inter-frame modeling during the preprocessing stage, it fails to genuinely enhance the temporal understanding capability of the LLM. Therefore, EventVAD incorporates temporal considerations for subsequent LLM scoring during event segmentation. Dividing long videos into coherent snippets, not only improves LLM comprehension but also enhances the model’s temporal reasoning capabilities.

Impact of Hyperparameters on Model Performance. EventVAD’s core hyperparameters - the temporal decay coefficient γ and semantic-motion fusion coefficient α - critically govern model behavior. We present a systematic analysis of their impacts.

As shown in Table 4, the temporal decay factor and the semantic-motion fusion coefficient have a serious impact on model behavior through their coordinated control of spatiotemporal feature integration. With the increase of γ and α , it is initially possible for the

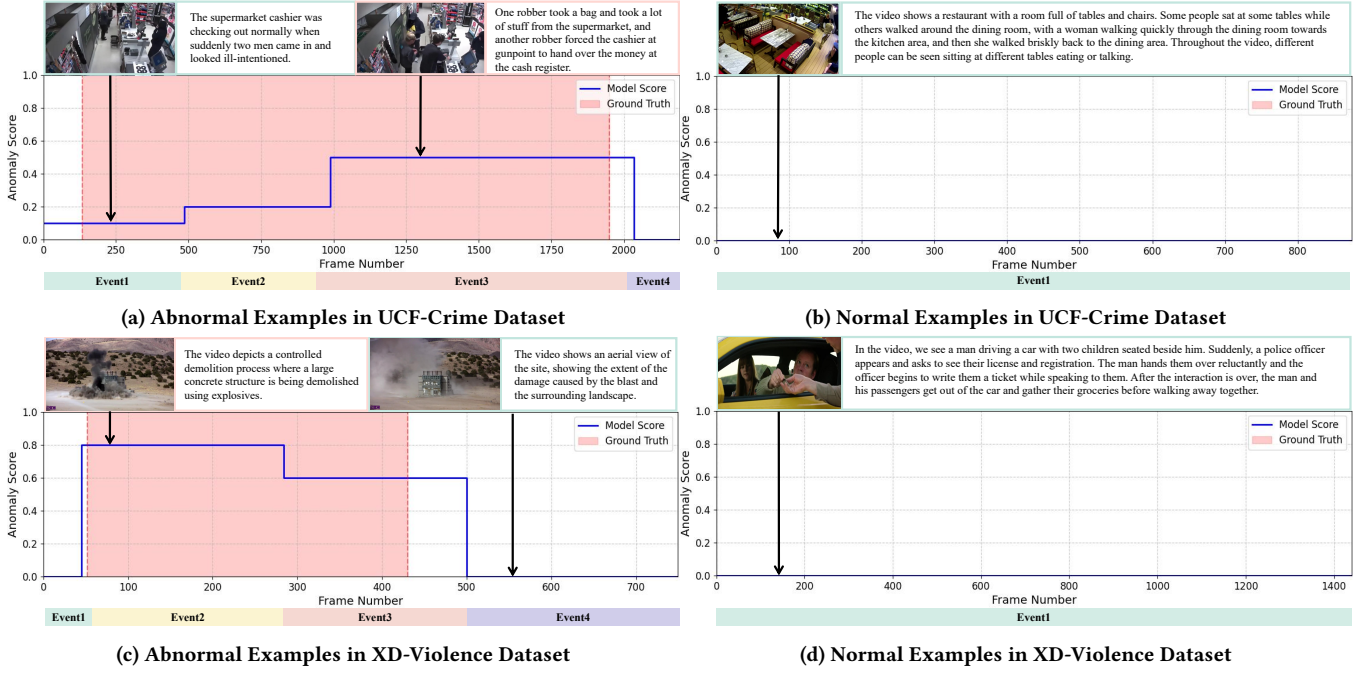


Figure 5: Visualization of normal and abnormal samples in the UCF-Crime and XD-Violence datasets. We visualized the samples which LAVAD failed to detect anomalies correctly. The figure presents event segmentation results along with the MLLM’s anomaly frame scores, with comparisons to the ground truth.

Method	Foundational Model	Parameters	AUC (%)
LAVAD [63]	Llama2-7b	7B	68.58
EventVAD (Ours)			78.39
LAVAD [63]	Llama2-13b	13B	78.33
EventVAD (Ours)			80.12
LAVAD [63]	Video-Llama2	7B	73.28
EventVAD (Ours)			82.03

Table 3: Effect of the parameter of the foundational model. EventVAD outperforms LAVAD in enhancing LLM scoring capabilities while demonstrating better compatibility with video LLMs.

	$\alpha = 0$	$\alpha = 0.25$	$\alpha = 0.5$	$\alpha = 0.75$	$\alpha = 1$
$\gamma = 0.0$	77.92	77.13	78.47	78.91	77.34
$\gamma = 0.2$	78.22	78.85	79.48	80.56	77.93
$\gamma = 0.4$	78.95	79.12	79.95	81.78	79.46
$\gamma = 0.6$	79.89	80.67	81.57	82.03	79.69
$\gamma = 0.8$	78.92	79.54	80.38	81.34	79.62
$\gamma = 1.0$	77.12	78.81	78.75	80.97	78.97

Table 4: Impact of Hyperparameters on EventVAD Performance. The experimental results demonstrate that our hyperparameter selection is reasonably well-justified.

framework to improve the quality of segmentation by enhancing the semantic correlation between frames while maintaining appropriate temporal continuity constraints. However, too high parameter values will lead to performance degradation, which will make the model overly sensitive to semantic changes, generate fragmented

RAFT	GANP	Thinking	AUC (%)	Δ (%)
✗	✗	✗	73.93	-
✗	✓	✗	77.81	+3.88
✓	✗	✗	75.35	+1.42
✓	✓	✗	80.14	+6.21
✗	✗	✓	75.64	+1.71
✗	✓	✓	79.97	+6.04
✓	✗	✓	76.86	+2.93
✓	✓	✓	82.03	+8.10

Table 5: Effect of different components on EventVAD. Through ablation studies of various components, we examine their contributions and identify the most critical ones.

fragments, and thus disrupt event continuity. These ultra-short fragments prevent MLLMs from establishing a full semantic context, resulting in hallucinogenic anomalous scoring.

To maintain a good semantic correlation between frames while having a certain time continuity constraint, we choose $\alpha = 0.75$ and $\gamma = 0.6$ for segmentation.

Key Component Ablation. For EventVAD, the Optical Flow Module, the Graph Attention propagation module, and the video content description before MLLMs scoring provide the main contribution to the model’s performance. To systematically evaluate each component’s contribution, we conducted modular ablation studies focusing on three key aspects: (1) the inclusion of RAFT-based optical flow features during encoding, (2) the use of graph attention network propagation (GANP) following dynamic graph construction,

and (3) the implementation of deliberative reasoning in MLLM outputs before anomaly scoring. We further analyzed cross-component interactions to explore potential synergies.

As shown in Table 5, when the original model is combined with the RAFT optical flow, the detection AUC increases by 2%, while with the help of graph attention propagation, the detection AUC of the model is further increased by about 4%. This is a significant improvement over static graphs and solves the problem of long graph neural network training times. Although RAFT optical flow cannot directly enhance the capabilities of the Dynamic Graph or Graph Attention Propagation modules, it can enhance the modeling capabilities of the Dynamic Graph through temporal feature matching, thereby improving its boundary detection performance. In addition, the quantitative experiments show the structured MLLM output can be specified, so that it can summarize the video content before outputting the abnormal score, and this process of letting the model think can better help him understand these small fragments and give a more reasonable score.

5 CONCLUSION

In this paper, we propose a novel training-free event-aware video anomaly detection framework, EventVAD. EventVAD addresses the challenge of localizing fine-grained visual transitions and diverse events in long videos by segmenting events in videos. EventVAD achieves more accurate event boundary detection and events division by introducing optical flow matching and dynamic graph architectures so that MLLMs can score anomalies accurately within events. We evaluated EventVAD on both UCF-Crime and XD-Violence datasets, experimental results demonstrate that EventVAD can segment events accurately in videos and achieves SOTA in video anomaly detection on both datasets in the training-free setting with 7B MLLMs compared to baseline 13B or larger MLLMs. The results also demonstrate that EventVAD outperforms unsupervised and one-class settings, which demonstrates that EventVAD exhibits strong generalization capabilities. So, this work makes a substantial contribution to the field by introducing a flexible and robust framework for video anomaly detection.

REFERENCES

- [1] Jean-Baptiste Alayrac, Jeff Donahue, Pauline Luc, Antoine Miech, Iain Barr, Yana Hasson, Karel Lenc, Arthur Mensch, Katherine Millican, Malcolm Reynolds, et al. 2022. Flamingo: a visual language model for few-shot learning. *Advances in neural information processing systems* 35 (2022), 23716–23736.
- [2] Kirolos Ataallah, Xiaoqian Shen, Eslam Abdelrahman, Essam Sleiman, Deyao Zhu, Jian Ding, and Mohamed Elhoseiny. 2024. Minigpt4-video: Advancing multimodal llms for video understanding with interleaved visual-textual tokens. *arXiv preprint arXiv:2404.03413* (2024).
- [3] Keqin Chen, Zhao Zhang, Weili Zeng, Richong Zhang, Feng Zhu, and Rui Zhao. 2023. Shikra: Unleashing multimodal llm's referential dialogue magic. *arXiv preprint arXiv:2306.15195* (2023).
- [4] Yingxian Chen, Zhengzhe Liu, Baoheng Zhang, Wilton Fok, Xiaojuan Qi, and Yik-Chung Wu. 2023. Mgf: Magnitude-contrastive glance-and-focus network for weakly-supervised video anomaly detection. In *AAAI*.
- [5] Zesen Cheng, Sicong Leng, Hang Zhang, Yifei Xin, Xin Li, Guanzheng Chen, Yongxin Zhu, Wenqi Zhang, Ziyang Luo, Deli Zhao, et al. 2024. Videollama 2: Advancing spatial-temporal modeling and audio understanding in video-llms. *arXiv preprint arXiv:2406.07476* (2024).
- [6] Prabhu Prasad Dev, Raju Hazari, and Pranesh Das. 2025. MCANet: Multimodal Caption Aware Training-Free Video Anomaly Detection via Large Language Model. In *International Conference on Pattern Recognition*. Springer, 362–379.
- [7] Jia-Chang Feng, Fa-Ting Hong, and Wei-Shi Zheng. 2021. Mist: Multiple instance self-training framework for video anomaly detection. In *CVPR*.
- [8] Rohit Girdhar, Alaeldin El-Nouby, Zhuang Liu, Mannat Singh, Kalyan Vasudev Alwala, Armand Joulin, and Ishan Misra. 2023. Imagebind: One embedding space to bind them all. In *CVPR*.
- [9] Aaron Grattafiori, Abhimanyu Dubey, Abhinav Jauhri, Abhinav Pandey, Abhishek Kadian, Ahmad Al-Dahle, Aiesha Letman, Akhil Mathur, Alan Schelten, Alex Vaughan, et al. 2024. The llama 3 herd of models. *arXiv preprint arXiv:2407.21783* (2024).
- [10] Mahmudul Hasan, Jonghyun Choi, Jan Neumann, Amit K Roy-Chowdhury, and Larry S Davis. 2016. Learning temporal regularity in video sequences. In *CVPR*.
- [11] Wenyi Hong, Weihang Wang, Ming Ding, Wenmeng Yu, Qingsong Lv, Yan Wang, Yean Cheng, Shiyu Huang, Junhui Ji, Zhao Xue, et al. 2024. Cogvlm2: Visual language models for image and video understanding. *arXiv preprint arXiv:2408.16500* (2024).
- [12] Bin Huang, Xin Wang, Hong Chen, Zihan Song, and Wenwu Zhu. 2024. Vtmellm: Empower llm to grasp video moments. In *Proceedings of the IEEE/CVF Conference on Computer Vision and Pattern Recognition*. 14271–14280.
- [13] Yang Jin, Zhicheng Sun, Kun Xu, Liwei Chen, Hao Jiang, Quzhe Huang, Chengru Song, Yuliang Liu, Di Zhang, Yang Song, et al. 2024. Video-lavit: Unified video-language pre-training with decoupled visual-motional tokenization. *arXiv preprint arXiv:2402.03161* (2024).
- [14] Yang Jin, Kun Xu, Liwei Chen, Chao Liao, Jianchao Tan, Quzhe Huang, Bin Chen, Chenyi Lei, An Liu, Chengru Song, et al. 2023. Unified language-vision pretraining in llm with dynamic discrete visual tokenization. *arXiv preprint arXiv:2309.04669* (2023).
- [15] Hyekang Kevin Joo, Khoa Vo, Kashu Yamazaki, and Ngan Le. 2023. CLIP-TSA: CLIP-Assisted Temporal Self-Attention for Weakly-Supervised Video Anomaly Detection. In *ICIP*.
- [16] Christophe Leys, Christophe Ley, Olivier Klein, Philippe Bernard, and Laurent Licata. 2013. Detecting outliers: Do not use standard deviation around the mean, use absolute deviation around the median. *Journal of experimental social psychology* 49, 4 (2013), 764–766.
- [17] Guoqi Li, Guanxiong Cai, Xingyu Zeng, and Rui Zhao. 2022. Scale-Aware Spatio-Temporal Relation Learning for Video Anomaly Detection. In *ECCV*.
- [18] Junnan Li, Dongxu Li, Silvio Savarese, and Steven Hoi. 2023. Blip-2: Bootstrapping language-image pre-training with frozen image encoders and large language models. In *ICML*.
- [19] Junnan Li, Dongxu Li, Caiming Xiong, and Steven Hoi. 2022. Blip: Bootstrapping language-image pre-training for unified vision-language understanding and generation. In *International conference on machine learning*. PMLR, 12888–12900.
- [20] Kunchang Li, Yali Wang, Yinan He, Yizhuo Li, Yi Wang, Yi Liu, Zun Wang, Jian Xu, Guo Chen, Ping Luo, et al. 2024. Mvbench: A comprehensive multi-modal video understanding benchmark. In *Proceedings of the IEEE/CVF Conference on Computer Vision and Pattern Recognition*. 22195–22206.
- [21] Shuo Li, Fang Liu, and Licheng Jiao. 2022. Self-training multi-sequence learning with transformer for weakly supervised video anomaly detection. In *AAAI*.
- [22] Minwen Liao, Hao Bo Dong, Xinyi Wang, Ziyang Yan, and Yihua Shao. 2025. GM-MoE: Low-Light Enhancement with Gated-Mechanism Mixture-of-Experts. *arXiv preprint arXiv:2503.07417* (2025).
- [23] Bin Lin, Yang Ye, Bin Zhu, Jiaxi Cui, Munan Ning, Peng Jin, and Li Yuan. 2023. Video-llava: Learning united visual representation by alignment before projection. *arXiv preprint arXiv:2311.10122* (2023).
- [24] Haotian Liu, Chunyuan Li, Yuheng Li, and Yong Jae Lee. 2023. Improved baselines with visual instruction tuning. *arXiv* (2023).
- [25] Haotian Liu, Chunyuan Li, Qingyang Wu, and Yong Jae Lee. 2023. Visual instruction tuning. *Advances in neural information processing systems* 36 (2023), 34892–34916.
- [26] Ruyang Liu, Chen Li, Haoran Tang, Yixiao Ge, Ying Shan, and Ge Li. 2024. St-llm: Large language models are effective temporal learners. In *European Conference on Computer Vision*. Springer, 1–18.
- [27] Cewu Lu, Jianping Shi, and Jiaya Jia. 2013. Abnormal event detection at 150 fps in matlab. In *ICCV*.
- [28] Muhammad Maaz, Hanoona Rasheed, Salman Khan, and Fahad Shahbaz Khan. 2023. Video-chatgpt: Towards detailed video understanding via large vision and language models. *arXiv preprint arXiv:2306.05424* (2023).
- [29] Rashmiranjan Nayak, Umesh Chandra Pati, and Santos Kumar Das. 2021. A comprehensive review on deep learning-based methods for video anomaly detection. *Image and Vision Computing* (2021).
- [30] Alec Radford, Jong Wook Kim, Chris Hallacy, Aditya Ramesh, Gabriel Goh, Sandhini Agarwal, Girish Sastry, Amanda Askell, Pamela Mishkin, Jack Clark, et al. 2021. Learning transferable visual models from natural language supervision. In *International conference on machine learning*. PMLR, 8748–8763.
- [31] Bharathkumar Ramachandra, Michael J Jones, and Ranga Raju Vatsavai. 2020. A survey of single-scene video anomaly detection. *IEEE transactions on pattern analysis and machine intelligence* 44, 5 (2020), 2293–2312.
- [32] Fabio Remondino, Ali Karami, Ziyang Yan, Gabriele Mazzacca, Simone Rigon, and Rongjun Qin. 2023. A critical analysis of NeRF-based 3D reconstruction. *Remote Sensing* 15, 14 (2023), 3585.
- [33] Franco Scarselli, Marco Gori, Ah Chung Tsoi, Markus Hagenbuchner, and Gabriele Monfardini. 2008. The graph neural network model. *IEEE transactions on neural networks* 20, 1 (2008), 61–80.
- [34] Yihua Shao, Siyu Liang, Zijian Ling, Minxi Yan, Haiyang Liu, Siyu Chen, Ziyang Yan, Chenyu Zhang, Haotong Qin, Michele Magno, et al. 2024. GWQ: Gradient-Aware Weight Quantization for Large Language Models. *arXiv preprint arXiv:2411.00850* (2024).
- [35] Yihua Shao, Deyang Lin, Fanhu Zeng, Minxi Yan, Muyang Zhang, Siyu Chen, Yuxuan Fan, Ziyang Yan, Haozhe Wang, Jingcai Guo, et al. 2025. TR-DQ: Time-Rotation Diffusion Quantization. *arXiv preprint arXiv:2503.06564* (2025).
- [36] Yihua Shao, Yeling Xu, Xinwei Long, Siyu Chen, Ziyang Yan, Yang Yang, Haoting Liu, Yan Wang, Hao Tang, and Zhen Lei. 2024. AccidentBlip: Agent of Accident Warning based on MA-former. *arXiv preprint arXiv:2404.12149* (2024).
- [37] Yihua Shao, Minxi Yan, Yang Liu, Siyu Chen, Wenjie Chen, Xinwei Long, Ziyang Yan, Lei Li, Chenyu Zhang, Nicu Sebe, et al. 2025. In-Context Meta LoRA Generation. *arXiv preprint arXiv:2501.17635* (2025).
- [38] Fahad Sohrab, Jenni Raitoharju, Moncef Gabbouj, and Alexandros Iosifidis. 2018. Subspace support vector data description. In *ICPR*.
- [39] Yixuan Su, Tian Lan, Huayang Li, Jialu Xu, Yan Wang, and Deng Cai. 2023. Pandagpt: One model to instruction-follow them all. *arXiv preprint arXiv:2305.16355* (2023).
- [40] Waqas Sultani, Chen Chen, and Mubarak Shah. 2018. Real-world anomaly detection in surveillance videos. In *CVPR*.
- [41] Quan Sun, Yuxin Fang, Ledell Wu, Xinlong Wang, and Yue Cao. 2023. Eva-clip: Improved training techniques for clip at scale. *arXiv preprint arXiv:2303.15389* (2023).
- [42] Zachary Teed and Jia Deng. 2020. Raft: Recurrent all-pairs field transforms for optical flow. In *Computer Vision—ECCV 2020: 16th European Conference, Glasgow, UK, August 23–28, 2020, Proceedings, Part II 16*. Springer, 402–419.
- [43] Kamalakar Vijay Thakare, Debi Prosad Dogra, Heeseung Choi, Haksun Kim, and Ig-Jae Kim. 2023. RareAnom: A Benchmark Video Dataset for Rare Type Anomalies. *Pattern Recognition* (2023).
- [44] Kamalakar Vijay Thakare, Yash Raghuvanshi, Debi Prosad Dogra, Heeseung Choi, and Ig-Jae Kim. 2023. DyAnNet: A Scene Dynamicity Guided Self-Trained Video Anomaly Detection Network. In *WACV*.
- [45] Yu Tian, Guansong Pang, Yuanhong Chen, Rajvinder Singh, Johan W Verjans, and Gustavo Carneiro. 2021. Weakly-supervised video anomaly detection with robust temporal feature magnitude learning. In *ICCV*.
- [46] Hugo Touvron, Thibaut Lavril, Gautier Izacard, Xavier Martinet, Marie-Anne Lachaux, Timothée Lacroix, Baptiste Rozière, Naman Goyal, Eric Hambro, Faisal Azhar, et al. 2023. Llama: Open and efficient foundation language models. *arXiv* (2023).
- [47] Anil Osman Tur, Nicola Dall'Asen, Cigdem Beyan, and Elisa Ricci. 2023. Exploring diffusion models for unsupervised video anomaly detection. In *ICIP*.
- [48] Anil Osman Tur, Nicola Dall'Asen, Cigdem Beyan, and Elisa Ricci. 2023. Unsupervised Video Anomaly Detection with Diffusion Models Conditioned on Compact Motion Representations. In *ICIAP*.
- [49] Ashish Vaswani, Noam Shazeer, Niki Parmar, Jakob Uszkoreit, Llion Jones, Aidan N Gomez, Łukasz Kaiser, and Illia Polosukhin. 2017. Attention is all you need. *NeurIPS* (2017).
- [50] Petar Veličković, Guillem Cucurull, Arantxa Casanova, Adriana Romero, Pietro Liò, and Yoshua Bengio. 2018. Graph Attention Networks. In *International Conference on Learning Representations*.

- [51] Jue Wang and Anoop Cherian. 2019. Gods: Generalized one-class discriminative subspaces for anomaly detection. In *ICCV*.
- [52] Weihang Wang, Qingsong Lv, Wenmeng Yu, Wenyi Hong, Ji Qi, Yan Wang, Junhui Ji, Zhuoyi Yang, Lei Zhao, Song XiXuan, et al. 2024. Cogvlm: Visual expert for pretrained language models. *Advances in Neural Information Processing Systems* 37 (2024), 121475–121499.
- [53] Jhih-Ciang Wu, He-Yen Hsieh, Ding-Jie Chen, Chiou-Shann Fuh, and Tyng-Luh Liu. 2022. Self-supervised Sparse Representation for Video Anomaly Detection. In *ECCV*.
- [54] Peng Wu and Jing Liu. 2021. Learning causal temporal relation and feature discrimination for anomaly detection. *IEEE TIP* (2021).
- [55] Peng Wu, Jing Liu, Yujia Shi, Yujia Sun, Fangtao Shao, Zhaoyang Wu, and Zhiwei Yang. 2020. Not only look, but also listen: Learning multimodal violence detection under weak supervision. In *ECCV*.
- [56] Ziyang Yan, Wenzhen Dong, Yihua Shao, Yuhang Lu, Liu Haiyang, Jingwen Liu, Haozhe Wang, Zhe Wang, Yan Wang, Fabio Remondino, et al. 2024. Renderworld: World model with self-supervised 3d label. *arXiv preprint arXiv:2409.11356* (2024).
- [57] Ziyang Yan, Lei Li, Yihua Shao, Siyu Chen, Zongkai Wu, Jenq-Neng Hwang, Hao Zhao, and Fabio Remondino. 2024. 3dsceneeditor: Controllable 3d scene editing with gaussian splatting. *arXiv preprint arXiv:2412.01583* (2024).
- [58] Ziyang Yan, Gabriele Mazzacca, Simone Rigon, Elisa Mariarosaria Farella, Pawel Trybala, Fabio Remondino, et al. 2023. NeRFBK: a holistic dataset for benchmarking NeRF-based 3D reconstruction. *International Archives of the Photogrammetry, Remote Sensing and Spatial Information Sciences* 48, 1 (2023), 219–226.
- [59] Ziyang Yan, Nazanin Padkan, Pawel Trybala, Elisa Mariarosaria Farella, and Fabio Remondino. 2025. Learning-Based 3D Reconstruction Methods for Non-Collaborative Surfaces—A Metrological Evaluation. *Metrology* 5, 2 (2025), 20.
- [60] Qinghao Ye, Haiyang Xu, Jiabo Ye, Ming Yan, Anwen Hu, HaoWei Liu, Qi Qian, Ji Zhang, and Fei Huang. 2024. mplug-owl2: Revolutionizing multi-modal large language model with modality collaboration. In *Proceedings of the IEEE/CVF conference on computer vision and pattern recognition*. 13040–13051.
- [61] Muhammad Zaigham Zaheer, Arif Mahmood, Marcella Astrid, and Seung-Ik Lee. 2020. Claws: Clustering assisted weakly supervised learning with normalcy suppression for anomalous event detection. In *ECCV*.
- [62] M Zaigham Zaheer, Arif Mahmood, M Haris Khan, Mattia Segu, Fisher Yu, and Seung-Ik Lee. 2022. Generative cooperative learning for unsupervised video anomaly detection. In *CVPR*.
- [63] Luca Zanella, Willi Menapace, Massimiliano Mancini, Yiming Wang, and Elisa Ricci. 2024. Harnessing large language models for training-free video anomaly detection. In *Proceedings of the IEEE/CVF Conference on Computer Vision and Pattern Recognition*. 18527–18536.
- [64] Fanhu Zeng, Zhen Cheng, Fei Zhu, Hongxin Wei, and Xu-Yao Zhang. 2025. Local Prompt: Extensible Local Prompts for Few-Shot Out-of-Distribution Detection. In *The Thirteenth International Conference on Learning Representations*.
- [65] Fanhu Zeng, Zhen Cheng, Fei Zhu, and Xu-Yao Zhang. 2025. Towards Efficient and General-Purpose Few-Shot Misclassification Detection for Vision-Language Models. *arXiv preprint arXiv:2503.20492* (2025).
- [66] Fanhu Zeng, Haiyang Guo, Fei Zhu, Li Shen, and Hao Tang. 2025. Parameter Efficient Merging for Multimodal Large Language Models with Complementary Parameter Adaptation. *arXiv preprint arXiv:2502.17159* (2025).
- [67] Fanhu Zeng, Hao Tang, Yihua Shao, Siyu Chen, Ling Shao, and Yan Wang. 2025. MambaIC: State Space Models for High-Performance Learned Image Compression. *arXiv preprint arXiv:2503.12461* (2025).
- [68] Fanhu Zeng and Deli Yu. 2024. M2M-TAG: Training-Free Many-to-Many Token Aggregation for Vision Transformer Acceleration. In *Workshop on Machine Learning and Compression, NeurIPS 2024*.
- [69] Fanhu Zeng, Fei Zhu, Haiyang Guo, Xu-Yao Zhang, and Cheng-Lin Liu. 2024. Modalprompt: Dual-modality guided prompt for continual learning of large multimodal models. *arXiv preprint arXiv:2410.05849* (2024).
- [70] Hang Zhang, Xin Li, and Lidong Bing. 2023. Video-llama: An instruction-tuned audio-visual language model for video understanding. *arXiv preprint arXiv:2306.02858* (2023).
- [71] Jiangong Zhang, Laiyun Qing, and Jun Miao. 2019. Temporal convolutional network with complementary inner bag loss for weakly supervised anomaly detection. In *ICIP*.
- [72] Jia-Xing Zhong, Nannan Li, Weijie Kong, Shan Liu, Thomas H Li, and Ge Li. 2019. Graph convolutional label noise cleaner: Train a plug-and-play action classifier for anomaly detection. In *CVPR*.
- [73] Bin Zhu, Bin Lin, Munan Ning, Yang Yan, Jiaxi Cui, HongFa Wang, Yatian Pang, Wenhao Jiang, Junwu Zhang, Zongwei Li, et al. 2023. Languagebind: Extending video-language pretraining to n-modality by language-based semantic alignment. *arXiv preprint arXiv:2310.01852* (2023).

A APPENDIX

A.1 Detail of Datasets

UCF-Crime is a real-world surveillance dataset of 1,900 untrimmed videos (128 hours) spanning 13 anomalous categories (e.g., assault, robbery, explosion) with only normal videos (950 videos) in the training set and normal videos (950 videos) in the test set. Each video has a resolution of 320×240 fps with frame-level anomaly labels.

XD-Violence is a multi-scenario anomaly detection dataset with 4,754 videos covering 6 violent behaviors (e.g., riots, car accidents, gun shootings). Videos were collected at 30 fps and 720p resolution from film, sports, and CCTV footage, with 3,958 videos in the training set and 796 videos in the test set.

A.2 Detail of Evaluation Metrics

For a frame-wise prediction score s_i and ground-truth binary label $y_i \in \{0, 1\}$, AUC-ROC is computed by integrating the true positive rate (TPR) over false positive rate (FPR) across thresholds:

$$\text{AUC} = \int_0^1 \text{TPR}(\tau) d\text{FPR}(\tau), \quad (15)$$

where τ denotes the classification threshold. AP summarizes the precision-recall curve as the weighted mean of precisions at each threshold:

$$\text{AP} = \sum_k (R_k - R_{k-1}) P_k, \quad (16)$$

with P_k and R_k being precision and recall at the k -th threshold. All indicators are split from official datasets using a specified evaluation toolkit to avoid implementation bias.

A.3 More Ablation Study Results

Efficiency-Accuracy Trade-off on XD-Violence Datasets. To investigate the impact of video quality on MLM scoring, we conducted additional ablation experiments on the XD-Violence dataset. As shown in Tab. 6, the results are similar to those on the UCF-Crime dataset, indicating that video quality has minimal impact on EventVAD scoring.

Method	Foundational Model	Parameters	AP (%)	AUC (%)
LAVAD [63]	Llama2-7b	7B	54.77	75.28
EventVAD (Ours)			61.03	83.46
LAVAD [63]	Llama2-13b	13B	60.02	82.89
EventVAD (Ours)			62.95	85.63
LAVAD [63]	Video-Llama2	7B	56.08	77.21
EventVAD (Ours)			64.04	87.51

Table 6: Effect of the parameter of the foundational model. The detection capability of the Video-LLaMA2-7b surpasses that of LLaMA2-13b.

Received 20 February 2007; revised 12 March 2009; accepted 5 June 2009